Finite element analysis of shear deformation in reinforced concrete shear-critical beams

Zheng Huang[a], Zhitao Lü[a], Shoutan Song[a], Yongming Tu[a*], Thomas Blanksvärd[b], Gabriel Sas[c], Lennart Elfgren[b]

[a] *School of Civil Engineering, Southeast University, 210096, Nanjing, China.*

[b] *Division of Structural Engineering, Luleå University of Technology, SE-971 87, Luleå, Sweden.*

[c] *Infrastructure, Materials and Structures, Norut, Narvik, N-8504, Narvik, Norway*

*Corresponding author. Tel.: +86 13851894854; E-mail: tuyongming@seu.edu.cn

Co-authors:

Zheng Huang	Tel. : +86 13276673703; E-mail: zheng.huang.china@hotmail.com
Zhitao Lü	Tel. : +86 18260031402; E-mail: luzhitao@seu.edu.cn
Shoutan Song	Tel. : +86 13605167197; E-mail: songshoutan@hotmail.com
Thomas Blanksvärd	Tel. :+46 (0)920 491642; E-mail: thomas.blanksvard@ltu.se
Gabriel Sas	Tel. : +46 (0)70 391 6552; E-mail: gabriel.sas@norut.no
Lennart Elfgren	Tel. : +46 (0)920 493660; E-mail: lennart.elfgren@ltu.se

Finite element analysis of shear deformation in reinforced concrete shear-critical beams

The objective of this paper was to study the contribution of shear deformation in reinforced concrete (RC) shear-critical beams. A 2D concrete material model based on smeared fixed crack was presented and incorporated into a commercial finite element (FE) software Abaqus. A method of calculating shear and flexure deformation separately out of total deformation in the shear span was presented and implemented into the FE analysis. Several experiments of RC shear-critical beams were simulated and good agreement between the experimental and numerical results was obtained in terms of total deformation, flexure deformation, shear deformation and crack patterns. The results show that after shear cracking, the contribution of shear deformation to total deformation increases rapidly. The shear span-to-depth ratio, the longitudinal reinforcement, the shear reinforcement and the load level could be the critical factor to influence the contribution of shear deformation. It appears that for RC shear-critical beams without shear reinforcement, the deformational behaviour is governed by flexure deformation. However, for RC beams with shear reinforcement, the contribution of shear deformation is not negligible after shear cracks develop. Moreover, the measuring method could also affect the measured shear deformation. Finally, future work on experimental investigation into this topic is recommended.

Keywords: shear deformation; reinforced concrete shear-critical beams; 2D concrete material model; finite element analysis;

1 Introduction

In the design of reinforced concrete (RC) beams, the deflection should be restricted to satisfy the serviceability limit state requirements. It is widely-accepted that the deformation of RC beams which are not subjected to axial load comprises flexure deformation and shear deformation. For the concrete beams with span-to-depth ratios larger than 10, the shear deformation is negligible prior to diagonal cracking (Timoshenko & Gere, 1972). However, after diagonal cracks form, the contribution of shear deformation is not negligible (Debernardi & Taliano, 2006; Hansapinyo, Pimanmas, Maekawa, & Chaisomphob, 2003; Pan, Li, & Lu, 2014; Ueda, Sato, Ito, & Nishizone, 2002)

The existing codes (AASHTO, 2007; ACI, 2014; CEN, 2004; FIB, 2010a) for concrete structures only provide formulas for estimating flexure deformation based on Navier-Bernoulli theory which could underestimate the deflection as a result of neglecting shear deformation (Desalegne & Lubell, 2012; Pan, et al., 2014).

Although extensive shear-failure experiments have been conducted on RC shear-critical beams (K. S. Kim, 2004), little attention has been paid to the shear deformation. To the authors' knowledge, the shear deformation of RC shear-critical beams was rarely measured separately out of the total deformation in existing experiments except for the following three. Ueda, et al. (2002) performed experiments of four rectangular RC beams with shear reinforcement in which the shear deformation in the shear span was measured by the laser speckle method. The experimental results suggested for rectangular RC beams, the shear deformation could account for 10% to 40% of the total deformation at half of the ultimate load and 30% to 60% at failure. Hansapinyo, et al. (2003) examined the shear deformation of four rectangular RC beams with shear reinforcement. Three measuring lattices were attached to the surface of the shear span to measure the shear deformation. The results indicated the shear-to-total deformation ratio could reach 20% to 30% at half of the ultimate load and 30% to 40% at failure. Debernardi and Taliano (2006) carried out experimental investigations into six RC beams with thin web and square lattices were used to measure the shear deformation in the shear span. It showed that 25% of the total deformation was comprised of shear deformation at the ultimate load in terms of RC beams with thin web. Large scatter could be found when it came to the measured shear deformation in those tests. The reason could be that the measured shear deformation was affected by many factors, such as the shear span-to-depth ratio, the reinforcement, the web width and the measuring method.

A number of theoretical investigations into this topic have also been conducted in the past few years. The truss analogy (Debernardi, Guiglia, & Taliano, 2011; J. H. Kim & Mander, 2007; Pan, et al., 2014; Ueda, et al., 2002; Wang, Dai, & Zheng, 2015) and the modified compression field theory (Desalegne & Lubell, 2012; Hansapinyo, et al., 2003; F. J. Vecchio & Collins, 1986) have been adopted to estimate the shear deformation in the shear span of RC beams. A theoretical and experimental study including time-dependent behaviour has been performed by (Jin, 2016).

The Finite Element Method (FEM) is a typical alternative of examining the performance of reinforced concrete structures to physical testing in a laboratory. The 2D FEM model with plane stress elements is suitable for simulating the shear behaviour of RC shear-critical beams and has been widely employed by other researchers (Bertagnoli & Carbone, 2008; J. Cervenka & Cervenka, 2010; V. Cervenka & Pukl, 1992; Coronelli & Mulas, 2006; FIB, 2010b; Maekawa, Pimanmas, & Okamura, 2003; Malm, 2006; Sato, Tadokoro, & Ueda, 2004; F. J. Vecchio & Shim, 2004). Nevertheless, all of these simulations were performed to investigate the shear capacity and the load-total deformation curve of RC shear-critical beams. Shear deformation has barely been extracted separately from total deformation in these FEM analyses to estimate its contribution.

In this paper, a 2D concrete material model based on smeared fixed crack model is presented and incorporated into the general-purpose FEM software Abaqus 6.10 (Hibbitt, 1997) through the subroutine interface VUMAT. Additionally, a method of separating flexure and shear deformation out of total deformation is presented and implemented in the FEM model. In order to validate the capability of this FEM model along with the deformation-separation method to reproduce the deformational behaviour of RC shear-critical beams, the results produced using this model are compared with those obtained from a number of well documented tests on RC beams conducted by different authors. The contributions of the shear deformation to the total deformation of these beam specimens are investigated. What's more, the influence of measuring methods on the experimental results of shear deformation is also discussed via the FEM analysis to guide the future experimental research.

2. Two-dimensional concrete material model

Three built-in material models are available for simulating concrete material in Abaqus 6.10, i.e.. Concrete Damaged Plasticity (CDP), Concrete Smeared Cracking (CSC) and Brittle Cracking (BC). According to the authors' investigation (Huang, Lü, & Tu, 2016; Huang et al., 2016), it appears that the damage evolution laws of the CDP model could influence the predicted shear behaviour of RC shear-critical beams but it was difficult to specify such laws which were capable of well predicting the real crack pattern and shear capacity of RC beams. When applying the CSC model to simulating RC shear-critical beams, convergence difficulties could always be encountered and it was hard to track the overall failure process. In terms of the BC model provided by Abaqus, the compression behaviour is assumed to be linear elastic which is not suited for modelling the RC shear-critical beams because significant compression stresses may develop in the concrete in this case and nonlinear compression behaviour will influence the performance of these beams. Hence, it is necessary to incorporate a reliable concrete material model to Abaqus which can well simulate RC shear-critical beams.

The proposed concrete material model was incorporated into Abaqus through the subroutine interface VUMAT. The concrete was treated as a nonlinear isotropic elastic material before cracking while the smeared fixed crack model based on the orthotropic material was used to model the post-cracking behaviour. For the sake of eliminating the effect of Possion's ratio on applying the uniaxial stress-strain curve to biaxial stress state, the concept of 'equivalent uniaxial strain' developed by Darwin and Pecknold (1977) was introduced in this model as shown:

$$\begin{bmatrix} \varepsilon_1^{eq} \\ \varepsilon_2^{eq} \\ \gamma_{12}^{eq} \end{bmatrix} = \begin{bmatrix} \frac{1}{1-\nu^2} & \frac{\nu}{1-\nu^2} & 0 \\ \frac{\nu}{1-\nu^2} & \frac{1}{1-\nu^2} & 0 \\ 0 & 0 & 1 \end{bmatrix} \begin{bmatrix} \varepsilon_1 \\ \varepsilon_2 \\ \gamma_{12} \end{bmatrix} \tag{1}$$

where ε_1 is the maximum principle strain for uncracked concrete or the strain normal to the fixed crack for cracked concrete, ε_2 is the minimum principle strain for uncracked concrete or the strain parallel to the crack for cracked concrete, γ_{12} is null for uncracked concrete or the shear strain along the crack for cracked concrete, the strain symbol with superscript 'eq' represents the corresponding equivalent uniaxial strain in which the Possion's ratio effect is removed and ν is Possion's ratio. According to the guidelines presented by Hendriks et al. (2012), ν was set to be equal to 0.2 for uncracked concrete and 0 for cracked concrete.

2.1 Stress-Strain Relationships

The expression of the stress-strain curve proposed by the fib Model Code 2010 (FIB, 2010a) was adopted for the ascending branch of concrete in compression：

$$\sigma = \beta_c f_c \left(\frac{k\eta - \eta^2}{1+(k-2)\eta} \right)$$
$$\eta = \frac{\varepsilon^{eq}}{\varepsilon_c} \tag{2}$$
$$k = \frac{E_c \varepsilon_c}{\beta_c f_c}$$

where f_c is the concrete cylinder compressive strength, ε_c is the strain at peak stress, E_c is the concrete elastic modulus and β_c is the coefficient of compressive strength aimed for taking the biaxial stress state into account which will be discussed below. f_c was determined according to the experiment while ε_c and E_c were estimated from the cylinder compressive strength according to Model Code 2010.

Compared to the ascending branch of the compressive stress-strain curve, it was much more complicated to define the compressive softening behaviour. In order to reduce the mesh size sensitivity during compressive strain localization, Nakamura (2001) proposed a model based on compressive fracture energy which was constant regardless of the size and the shape of the specimen. What's more, due to lateral confinement, the presence of in-plane and out-of-plane reinforcement could enhance the ductility of concrete which also had some influence on the compressive descending branch (Bertagnoli, Mancini, Recupero, & Spinella, 2011; Kent & Park, 1971). J. Cervenka and Cervenka (2010) also presented a compressive softening model based on compressive fracture energy as shown in Equation (3). In this equation, the end point of the softening curve was defined by w_d (in mm), termed as the value of the plastic end displacement. Under this way, the compressive fracture energy was defined. According to the experimental investigation into the compressive behaviour of concrete performed by Van Mier (1986), the value of w_d could be taken as 0.5mm. J. Cervenka and Cervenka (2010) simulated a RC shear-critical beam without shear reinforcement with good accuracy by taking the value of w_d as 0.5mm. However if using the same value for another beam with shear reinforcement, the peak load was underestimated. In order to obtain a best-fit response, the value of w_d was adjusted to 50mm. The reason might be that for RC shear-critical beams containing shear reinforcement which failed in the mode of shear-compression, the crushing of concrete around the loading plate was a critical factor. Therefore, it was necessary to consider the ductility enhancement of concrete compressive softening caused by the restraining effect of the loading plate (Bertagnoli, et al., 2011; F. J. Vecchio & Shim, 2004). In this study, the compressive descending stress-strain relationship was defined as a linear softening law following that proposed by J. Cervenka and Cervenka (2010):

$$\sigma = \beta_c f_c \left(-\frac{1}{w_d / l_c} \varepsilon^{eq} + \frac{\varepsilon_c}{w_d / l_c} + 1 \right) \tag{3}$$

where w_d is the plastic end displacement and l_c is the characteristic length. The concept of this model was analogous to the crack band theory (Bazant & Oh, 1983) and l_c was taken as $\sqrt{2A}$ as recommended by Rots (1988), where A is the area of the element. ε_c+w_d/l_c represents the ultimate strain where the compressive stress is zero as shown in Figure 1. The value of w_d had to be calibrated for modelling different RC shear-critical beams on the basis of the aforementioned discussion. In this paper, this value was calibrated to 5 for all the beams with shear reinforcement and 0.5 for the beams without shear reinforcement studied in Section 4.

Before cracking, the behaviour of concrete subjected to tension was assumed to be linear elastic:

$$\sigma = E_c \varepsilon^{eq} \quad \sigma < \beta_t f_t \tag{4}$$

where f_t is the tensile strength of concrete derived from f_c according to Model Code 2010 and β_t is the coefficient of concrete tensile strength in biaxial stress state.

For the purpose of mitigating the mesh size sensitivity caused by tension softening, the stress-crack opening displacement curve proposed by Model Code 2010 was used to describe the post-cracking behaviour of concrete in tension:

$$\begin{aligned}
&\sigma = \beta_t f_t \left(1 - 0.8\frac{w}{w_1}\right) && w \le w_1 \\
&\sigma = \beta_t f_t \left(0.25 - 0.05\frac{w}{w_1}\right) && w_1 < w \le w_c \\
&w_1 = \frac{G_F}{f_t} && \\
&w_c = 5 \cdot \frac{G_F}{f_t} &&
\end{aligned} \tag{5}$$

where w is the crack opening displacement which is equal to $(\varepsilon^{eq}-\sigma/E_c)l_c$ according to the crack band theory, w_1 is the displacement when $\sigma=0.2\beta_t f_t$ and w_c is that when $\sigma=0$. The tensile strength f_t was estimated according to the Model Code 2010 while the tensile fracture energy G_F was calculated according to CEB-FIP Model Code 1990 (CEB-FIP, 1993) which is shown below because that calculated from Model Code 2010 could be excessively high (Hendriks, et al., 2012).

$$G_F = \left(0.0469 d_a^2 - 0.5 d_a + 26\right)\left(\frac{f_c}{10}\right)^{0.7} \tag{6}$$

where d_a is the maximum aggregate size. If no experimental value of this parameter was provided, d_a was assumed to be 20mm.

2.2 Uncracked Concrete

The biaxial failure criteria proposed by Kupfer and Gerstle (1973) was used to describe the failure criteria of uncracked concrete. This envelope is shown in Figure 2. For the uncracked concrete in the biaxial compression state, the enhancement of compressive strength was taken into account by defining the corresponding coefficient of compressive strength β_c which was calculated:

$$\beta_c = \frac{1+3.65\alpha}{\left(1+\alpha\right)^2} \qquad \alpha = \frac{\sigma_1}{\sigma_2} \tag{7}$$

where σ_1 and σ_2 is the maximum and minimum principal stress respectively. For uncracked concrete under tension-compression, the presence of compressive stress could reduce the tensile strength in the orthogonal direction which was considered by defining the corresponding coefficient of tensile strength β_t using the following formula:

$$\beta_t = 1 - 0.8\frac{\sigma_2}{f_c} \tag{8}$$

In the tension-tension state, it was assumed the tensile strength kept constant for both two principal directions as recommended by Kupfer and Gerstle (1973).

The stiffness matrix for uncracked concrete was in the form of a nonlinear isotropic elastic material as shown below:

$$\left[D\right] = \frac{E_{\mathrm{sec}}}{1-\nu^2}\begin{bmatrix} 1 & \nu & 0 \\ \nu & 1 & 0 \\ 0 & 0 & \frac{1-\nu}{2} \end{bmatrix} \tag{9}$$

where [D] is the stiffness matrix and E_{sec} is the nonlinear secant modulus determined from the uniaxial stress-strain curve in the minimum principal stress direction.

2.3 Cracked Concrete

For the cracked concrete, a smeared fixed crack model based on an orthotropic constitutive law was adopted. According to the RC shear panel experiments performed by F. Vecchio (1982) and Belarbi and Hsu (1995), the compressive strength could be weakened by the orthogonal tensile strain. Hendriks, et al. (2012) suggested that this tension-compression interaction should be taken into consideration to avoid the non-conservative estimation. In this paper, the reduction of compressive strength induced by parallel cracks was described by the formula proposed by F. Vecchio and Collins (1993):

$$\beta_c = \frac{1}{1+0.27\left(\frac{\varepsilon_1^{eq}}{\varepsilon_c}-0.37\right)} \tag{10}$$

The shear retention factor, representing the degradation of shear transfer across the cracks, is the ratio of secant shear modulus of cracked concrete to the elastic shear modulus of concrete before cracking. A variable shear retention factor was preferred instead of a constant to avoid the stress-locking phenomenon in which spurious principal stresses and an over-stiff response may be produced (Crisfield & Wills, 1989; Hendriks, et al., 2012; Rots, 1988). Many variable shear retention factor models dependant on the crack normal strain or/and the crack shear strain have been presented (Bazant & Gambarova, 1980; J. Cervenka & Cervenka, 2010; V. Cervenka, 1985; Maekawa, et al., 2003; Rots, 1988; Zhu, Hsu, & Lee, 2001). Although this factor has a significant influence on the predicted behaviour of cracked concrete, there is no widely-accepted model for it. In this paper, the variable shear retention factor model was used as proposed by Hendriks, et al. (2012), and J. Cervenka and Cervenka (2010) in which the secant shear stiffness decreased following the degradation of the secant tensile stiffness normal to the crack:

$$\beta_G = \frac{G_{cr}}{G + G_{cr}}$$
$$G_{cr} = s_F \frac{\sigma(w_{\max})}{\varepsilon_{\max}} \tag{11}$$

where β_G is the shear retention factor, G_{cr} is the secant shear modulus of cracked concrete, G is the elastic shear modulus of concrete, $\sigma(w_{max})$ is the tensile stress normal to the crack at the maximum crack opening displacement ever reached during the loading process calculated based on the tension softening law shown in Equation (5), ε_{max} is maximum crack opening strain ever reached during the loading process which can be taken as w_{max}/l_c according to the crack band theory and s_F is the scaling factor. The recommended value of s_F was within the range of 1-10 according to J. Cervenka and Papanikolaou (2008). However, in order to well simulate the behaviour of one RC beam without shear reinforcement and one with shear reinforcement, the values of s_F were set to be equal to 20 and 300 respectively by J. Cervenka and Cervenka (2010). It seems that the estimation of this value is strongly dependent on the reinforcement arrangement and maybe some other design parameters of RC structures. In this study, the value of s_F was calibrated to 125 for all the beams studied in Section 4.

The shear strength at the crack also needed to be defined as can be found in the existing models of shear stress transfer across the crack (or aggregate interlock models) (Bazant & Gambarova, 1980; Maekawa, et al., 2003; F. J. Vecchio, 2004). In this paper, the shear strength at the crack was estimated from the equation proposed in the Modified Compression Field Theory MCFT (Bentz, Vecchio, & Collins, 2006) which was also adopted by J. Cervenka and Cervenka (2010):

$$\tau_u = \frac{0.18\sqrt{f_c}}{0.31 + \frac{24w}{d_a + 16}} \tag{12}$$

where f_c in MPa, w and d_a in mm.

The stiffness matrix based on the orthotropic model (F. J. Vecchio, 1989) was used for the cracked concrete:

$$[D]=[T]^T[D_{cr}][T] \tag{13}$$

where $[D]$ is the stiffness matrix, $[D_{cr}]$ is the stiffness matrix at the local coordinate of cracks and $[T]$ is the transformation matrix. As presented above, the Possion's ratio for concrete after cracking was assumed to be zero. Thus, the $[D_{cr}]$ was given:

$$[D_{cr}]=\begin{bmatrix} E_1 & 0 & 0 \\ 0 & E_2 & 0 \\ 0 & 0 & \beta_G G \end{bmatrix} \tag{14}$$

where E_1 is the secant modulus for the direction normal to the crack, E_2 is the secant modulus for the direction parallel to the crack and $\beta_G G$ is the degraded shear modulus for describing the shear behaviour of the crack. In terms of the fixed crack model, the direction of crack propagation remained fixed after initial cracking. Hence, the transformation matrix $[T]$ remained constant as given below:

$$[T]=\begin{bmatrix} \cos^2\theta & \sin^2\theta & \cos\theta\sin\theta \\ \sin^2\theta & \cos^2\theta & -\cos\theta\sin\theta \\ -2\cos\theta\sin\theta & 2\cos\theta\sin\theta & (\cos^2\theta-\sin^2\theta) \end{bmatrix} \tag{15}$$

where θ is the angle between the cracks and the longitudinal direction of the beam.

3. Finite element model

The concrete was modelled using the plane stress element CPS4R in Abaqus and the reinforcement modelled by the truss element. Elastic-perfectly plastic material was applied to the reinforcement with the yield stress determined from the experiments and the elastic modulus taken as 200,000MPa. Perfect bond was assumed for describing the concrete-reinforcement interaction. In order to reduce the computational time, only half of the beams were built to take advantage of the symmetry if any. The steel plates at the supports and the loading points were included in the FEM model to distribute the stress caused by the concentrated load. The linear elastic materials with the elastic modulus of 200,000MPa and the Poisson's ratio 0.3 were used to model the steel plates.

With the aim of overcoming the convergence difficulty in modelling the propagation of cracks in concrete, the explicit dynamic solution approach provided by Abaqus was adopted. In the explicit dynamics procedure, the total step time is divided into a large number of small time increments and the explicit central difference method is used to conduct time integration (Chen, Teng, Chen, & Xiao, 2015; Hibbitt, 1997). Each increment is computationally inexpensive because neither iteration nor inversion of matrix needs to be done so that it often results in an economical computation. This integration method is conditionally stable and each time the increment should be smaller than the stability limit to produce a reasonable result. The value of the time increment can be automatically calculated in Abaqus and satisfactory results can be obtained using this value according to the authors' investigation. Moreover, the dynamic effect should be avoided in applying the dynamic analysis procedure to simulating static structural responses. In order to control this effect, the loading time should be sufficiently large and $100T_1$ is suitable for this parameter according to Chen, et al. (2015) where T_1 is the period of the fundamental vibration mode of the beam. Detailed information about applying explicit dynamic to quasi-static analysis of RC beams can be found in (Chen, et al., 2015).

4. Validation of the proposed model and calculation of shear and flexure deformation

Three groups of experiments on RC shear-critical beams conducted by different authors were studied in this section. The first group contained one I-section beam tested by Debernardi and Taliano (2006). The second group was comprised of four rectangular beams tested by Hansapinyo, et al. (2003). Experimental results in these two groups included measures of total deformation, flexure deformation and shear deformation. These beam specimens were chosen in order to validate the proposed FEM model and the method of calculating flexure and shear deformation presented in Section 4.1. The third group of experiments, carried out by Bresler and Scordelis (1963), consisted of 8 RC beams with rectangular cross sections. These specimens were commonly regarded as a benchmark against which FEM models could be calibrated and validated (Bertagnoli, et al., 2011). Moreover, These tests proved to be repeatable according to the duplicate beams tested by F. J. Vecchio and Shim (2004). The load-total deformation curves and crack pattern were reported by the authors while the shear deformation was not measured. In this paper, the total deformation and crack patterns were compared against the experimental observation and in addition, the contribution of shear deformation was estimated using the FEM model and the deformation-separation method presented in Section 4.1.

4.1 A method of calculating flexure and shear deformation in the FEM model

The method of extracting the shear deformation in the shear span of RC beams separately out of the total deformation in the FEM model was presented in this section. According to the finite element theory, the shear strain at the centre of a first-order four-nodes rectangular element and the corresponding shear deformation of this element can be calculated:

$$\gamma_e = \frac{u_1 + u_4 - u_2 - u_3}{2h} + \frac{v_3 + v_4 - v_1 - v_2}{2a} \tag{16}$$

$$\delta_s = a \cdot \gamma_e$$

where γ_e is the shear strain at the centre of the element, u_i is the displacement in the x direction of i^{th} node while v_i is that in the y direction, h and a are the height and the length of the element respectively, and δ_s is the shear deformation. All the variables above are illustrated in Figure 3(a). Figure (b) shows a schematic diagram of one half of one RC beam subjected to three point loads. The shear span of this beam could then be divided into several such macro-elements. Thus, the shear deformation at the loading point (or the end of the shear span) could be obtained by integrating the shear deformation of all these macro-elements.

The flexure deformation in the shear span was calculated on the basis of these macro-elements as well. Firstly, the mean curvature of the element was calculated:

$$\kappa_e = \frac{u_1 - u_4 + u_3 - u_2}{a \cdot h} \tag{17}$$

where κ_e is the mean curvature of the element. The rotation angle of each marco-element arising from the curvature was calculated by assuming constant curvature in each element:

$$\theta_e = a \cdot \kappa_e \tag{18}$$

where θ_e is the rotation angle of each element. Considering that the rotation angle atmid-span was zero, the rotation angle at the support could be obtained:

$$\theta_{\text{support}} = -\sum_{i=1}^{n} \theta_e^i \tag{19}$$

where $\theta_{support}$ is the rotation angle at the support, θ_e^i is the rotation angle of the i^{th} macro-element and n is the number of the macro-elements within the shear span. Finally, the flexure deformation at the right-most of the i^{th} macro-element was calculated using the following recursion formulas:

$$\begin{gathered} \delta_f^i = \delta_f^{i-1} + \theta^i a + \frac{1}{2}\kappa_e^i a^2 \\ \theta^i = \theta^{i-1} + \theta_e^{i-1} \\ \delta_f^0 = 0 \\ \theta^0 = \theta_{\text{support}} \\ \theta_e^0 = 0 \end{gathered} \tag{20}$$

where δ_f^i is the flexure deformation at the right-most of the i^{th} macro-element, θ^i is the cumulated rotation angle at the left-most of the i^{th} macro-element. In this way, the flexure deformation in the shear span was obtained.

In this paper, the above method of calculating shear and flexure deformation was implemented in the FEM model by which the contribution of shear deformation to total deformation can be quantified as shown in the following sections.

4.2 Debernardi-Taliano (DT) and Hansapinyo-Pimanmas (HP) Beams

In this section, the proposed model was used to simulate one I-section RC beams tested by Debernardi and Taliano (2006) and four rectangular beams tested by Hansapinyo, et al. (2003). All these beams were simply supported. The loading arrangements and geometry are shown in Figure 4. Table 1 lists the details of these beams and Table 2 provides the material properties of the reinforcement.

For DT-TR6, the shear span-to-depth ratio of the shorter shear span was 4.1. 500mm×500mm square lattices were used to measure the shear deformation. Instead of measuring the shear deformation along the beam axis continuously, square lattices were placed at several zones of different moment-to-shear ratio in the beam as depicted in

Figure 4. In order to obtain the contribution of the shear deformation to the total deformation at the load point, the experimental mean curvatures along the beam axis were recorded and integrated to estimate the flexure deformation. Then, the shear deformation was calculated by subtracting the flexure deformation from the total deformation. It should also be noted that only the cubic strength of concrete was provided for DT-TR6 in the original paper. In this paper, the cylinder strength of this beam was assumed to be 0.85 times the cubic strength.Hansapinyo, et al. (2003) tested four rectangular beams to study the following factors which could influence the shear deformation: the shear span-to-depth ratio, the longitudinal reinforcement and the shear reinforcement. Three measuring grids were used to cover the shear span to experimentally obtain the contribution of shear deformation to total deformation in the shear span.

In order to test the mesh sensitivity of this proposed model in simulating RC shear-critical beams, square or nearly square elements of different sizes were adopted. Figure 5 illustrates the numerical load-displacement curves of DT-TR6 using elements of sizes from 80mm to 20mm. It suggested that the use of elements of different sizes led to little variance in the simulated behaviour due to the fracture-based softening branch adopted in the proposed concrete model. This conclusion holds true for all beam specimens studied in this paper. The mesh size of 10mm was selected for all beams studied in this paper except for DT-TR6. Instead, the mesh size of 20mm was chosen for DT-TR6 to save computational time because of its fairly large size.The method of calculating shear deformation in the FEM model presented in the previous section was implemented in these beams. Before applying such method, the influence of the number of macro-elements that the shear span was divided into was investigated. Theoretically speaking, as the number of macro-elements increases, the measured shear deformation will converge as this method is analogous to the finite element method. Figure 6 compares the calculated contributions of the shear deformation of DT-TR6, HP-S1, HP-S2 with different numbers of such macro-elements. The *x*-axis represents the ratio of the calculated shear deformation to the calculated total deformation and the *y*-axis represents the applied load. The shear span-to-height ratio (*a/h*) of these three beams were 3.8, 2.3 and 3.0 respectively. It appears that the calculated shear deformation would converge after the selected number of macro-elements exceeded the value of *a/h*. In the experimental investigation performed by Hansapinyo, et al. (2003), the number of measuring lattices in the shear span was 3 which agreed with the above conclusion. However, if the shear span was divided into only one macro-element, the calculated shear deformation was significantly larger than the converged result. In the experiment conducted by Ueda, et al. (2002) , the value of *a/h* of the beam specimens was 2 but the experimental shear deformation was calculated by the measured displacement of four corners of the shear span using the laser speckle method which was just the same as dividing the shear span into only one macro-element. Hence, the shear deformation could be overestimated in their experimental investigation according to the above discussion.

Figure 7 shows the experimental results of the total deformation, the flexure deformation and the shear deformation at the load point for DT-TR6. Using the FEM model and the deformation-separation method mentioned above, the deformational results were also obtained numerically. It can be seen in this figure that if the shrinkage was omitted in the model, the three deformational results could all be underestimated. Investigations conducted by some researchers (Gribniak, Cervenka, & Kaklauskas, 2013; Kaklauskas, Gribniak, Bacinskas, & Vainiunas, 2009) indicated that the shrinkage of concrete might significantly influence cracking loads and flexure deformations of RC members subjected to short-term loading. To the authors' knowledge, no investigation concerning the effect of shrinkage on shear deformation has been performed. In this paper, the shrinkage effect was taken into account in the FEM model by applying initial strain to the concrete before loading. As the original paper didn't report the shrinkage strain, a typical value of -200$\mu\varepsilon$ for concrete at 28 days suggested by Kaklauskas, et al. (2009) was assumed in the simulation. As shown in Figure 7, by introducing the shrinkage, the cracking load was reduced. It was because the reinforcement could restrain the shrinkage of concrete which resulted in initial tension strain prior to loading. Using the FEM model with shrinkage considered, accuracy of the predictions improved not only for flexure deformation but also for shear deformation and total deformation.

Figure 8 compares the calculated deformational behaviour with the experimental results of HP series beams. A shrinkage strain of -200$\mu\varepsilon$ was also applied in the simulations. Note that for HP beams, the elastic modulus of concrete was estimated using the expression specified by ACI (2014) (i.e., $E_c=4700\sqrt{f_c}$) which was smaller than that proposed by FIB (2010a) to fit the experimental results. It was reasonable because the modulus of elasticity for concrete is not only dependent on the concrete strength but also sensitive to the modulus of elasticity of aggregate and mixture proportions of concrete. These details were not reported in the original paper. It can be seen in Figure 8 that the proposed FEM model also satisfactorily simulated the total deformation, the flexure deformation and the shear deformation of HP series beams,.

Figure 9 compares the calculated flexure deformation and shear deformation of HP beams. The shear cracking load was achieved from the experimental observation while the flexure cracking load was obtained from the numerical analysis. HP-S1 and HP-S2 had identical design parameters except for the value of *a/d*. As can be found in

Figure 9, both the shear deformation and flexure deformation of HP-S2 with larger *a/d* were larger than those of HP-S1. With the aim of studying the effect of longitudinal reinforcement, the response of HP-S1 and HP-S3 were compared. HP-S1 contained longitudinal reinforcement twice as much as HP-S3. As shown in Figure 9(a), after flexure cracking, HP-S3 had larger flexure deformation than HP-S1. Moreover, the amount of longitudinal reinforcement also had effects on the shear deformation as can be seen in Figure 9(b). Less longitudinal reinforcement (i.e. HP-S3) resulted in larger crack width which could reduce the shear stiffness as mentioned in Section 2. HP-S3 and HP-S4 only differed in the amount of shear reinforcement. No obvious difference could be observed with respect to the flexure deformation in Figure 9(a). As shown in Figure 9(b) the shear deformation of these two specimens were similar before shear cracking. After the shear cracks formed, the shear deformation of HP-S4 with smaller amount of shear reinforcement increased more rapidly than that of HP-S1. Similar discussion about the comparison of HP series beams can also be found in Hansapinyo, et al. (2003).

Figure 10 depicts the calculated contributions of shear deformation for DT and HP beams. The flexure cracking load and shear cracking load of DT-TR6 were both achieved from the experiment. At the elastic stage, the shear-to-total deformation ratio remained constant and the value ranged from 5 to 10 for different beams, depending on different shear span-to-depth ratios. At the onset of flexure cracks, this ratio decreased slightly because of the degradation of flexure stiffness induced by flexure cracking. Then, before shear cracking, the ratio began increasing after passing a turning point. It was attributed to the fact that the growth of the width of flexure cracks could degrade the shear transfer across the cracks as mentioned in the above paragraph and in Section 2. However, in general, during the phase between shear cracking and flexure cracking, the contribution of shear deformation didn't vary significantly compared to that at the elastic stage. After the shear cracks developed, the increase of the shear deformation was faster than that of the flexure deformation and the shear-to-total deformation ratio kept rising. For DT-TR6, the shear-to-total deformation ratio was 18% at 60% of the peak load and over 20% after the load level exceeded 80% of the peak load. For HP series beams, this ratio ranged from 12% to 18% at 60% of the peak load and exceeded 20% over 80% of the peak load. It can be seen in Figure 10(b) that for the lower longitudinal reinforcement ratio, the lower shear reinforcement ratio, the lower shear span-to-depth ratio and the higher load level, the contribution of shear deformation could be more significant.

4.3 Bresler-Scordelis (BS) Beams

In this section, the simulated results of eight RC shear-critical beams tested by Bresler and Scordelis (1963) were presented. The failure mode of beams containing no shear reinforcement(e.g. BS-OA1, BS-OA2) was diagonal-tension while that of the others with shear reinforcement was shear-compression. These beams were simply supported under three point loads and differed in the shear span-to-depth ratio, the amount of reinforcement and the beam width. The details are given in Table 1 and the material properties of the reinforcement are listed in Table 2. Figure 11 provides the schematic diagrams of the cross section and elevation of three typical BS series beams (e.g. BS-OA1, BS-B1, BS-C2).

Figure 12 shows the curves of the applied load versus mid-span displacement of all the eight beams from both experiments and numerical simulations. Figure 13 illustrates the comparison of the crack patterns at failure obtained numerically and experimentally. It should be noted that in simulating the BS beams, no shrinkage strain was applied to the concrete prior to loading. The calculated load-displacement curves showed good agreement with the experiments. The reason might be that all BS beams were tested at fairly young age (13 days after being cast) (Bresler & Scordelis, 1963) when no significant shrinkage strain may have developed in the concrete.

For beams containing no shear reinforcement, which was controlled by diagonal tension, failure was sudden after the formation of the 'critical diagonal tension crack' as observed in the experiments (Bresler & Scordelis, 1963). This crack also propagated to the compression zone and the bottom reinforcement near the end of the beam developing into longitudinal splitting finally. As shown in Figure 12 and Figure 13, the crack pattern at failure, as well as the overall load-displacement response, produced by the FEM model with the calibrated parameters are in good agreement with experimental observations.

For beams with shear reinforcement, the shear-compression failure was characterized by concrete crushing in the compression zone but without splitting along the bottom reinforcement (Bresler & Scordelis, 1963). These beams failed at loads greater than those at which the first diagonal crack emerged. The satisfactory simulations of load-displacement curves and crack patterns were obtained as shown in Figure 12 and Figure 13 in comparison with the experiments.

The method of separating shear and flexure deformation mentioned in Section 4.1 was implemented in BS series beams. The number of macro-elements was selected based on the relevant discussion in Section 4.2. Figure 14 shows the calculated contributions of the shear deformation of BS-OA2 and BS-A2 along with the flexure cracking load obtained from the FEM analysis and the shear cracking load from experiments. Note that in Figure 14, 15 and 16, the y axis represents the ratio of the applied load to the experimental peak load instead of the value of the applied load. These two beams were similar in all aspects, except that BS-A2 contained shear reinforcement while BS-OA2 did not. It can be seen in Figure 14 that at the beginning of the loading procedure, the shear deformation accounted for only around 5% of the total deformation for both two beams due to their similar geometry. After flexure cracking, the contribution of shear deformation declined first and then started to rise after passing a turning point below the shear cracking load. This phenomenon was similar with that of the above specimens and was also observed in all other BS series beams. Then, after shear cracking, the shear-to-total deformation ratio increased as the load level rose. Before 80% of the peak load, this ratio increased slowly and ranged from 4% to 5%. However, for BS-A2, after the applied load exceeded this level, this ratio went up to over 10% near failure. Whereas for BS-OA2 without shear reinforcement, this ratio remained almost constant during the overall loading procedure. It was because, in terms of shear-critical beams without shear reinforcement, the 'critical diagonal cracks' formed at a load quite close to the ultimate load before which no evident shear cracks could be found (Bresler & Scordelis, 1963). Namely, the shear cracking load was close to the peak load. Hence, the deformation of RC shear-critical beams without reinforcement is governed by flexure while shear deformation is negligible.

Figure 15 shows the calculated shear deformation for BS-B1 and BS-B2. All the design parameters of these two beams were the same except for the shear span-to-depth ratio (3.9 for BS-B1 and 4.9 for BS-B2). The results indicated that at the elastic stage, the ratio of shear-to-total deformation of BS-B1 (about 7%) was slightly larger than that of BS-B2 (about 5%) due to its smaller shear span-to-depth ratio. This difference became even larger over 80% of the ultimate load. The ratio of the shear-to-total deformation for BS-B1 was 10% at 80% of the peak load and more than 25% at ultimate load while for BS-B2, the corresponding value was 5% at 80% of the peak load and less than 10% at failure.

Among all BS series beams studied in this section, BS-C1 had the largest contribution of shear deformation. Despite of the fairly large shear-to-total deformation ratio at a higher load level (e.g. over 80% of the peak load), the corresponding value for BS-C1 at the service load (assumed to be 60% of the peak load) was 9.5% which was only slightly larger than that of 7.7% at the elastic stage as shown in Figure 16. It was because that the shear cracking load was quite close to the service load level which meant the shear stiffness didn't degrade significantly at the service load. Compared to BS-C1, DT-TR6 had similar shear span-to-depth ratio (4.1 vs 3.9) and longitudinal reinforcement ratio (1.57% vs 1.48%) while contained even more shear reinforcement (0.51% vs 0.20%). The shear-to-total deformation ratio for DT-TR6 was lower than that for BS-BC1 at the elastic stage. However, this ratio at the service load for DT-TR6 was nearly twice as much as that for BS-C1. It was attributed to its relatively low level of shear cracking load as shown in Figure 16. The shear cracks in DT-TR6 developed at only 20% of the peak load which meant at the service load (60% of the peak load), the shear stiffness could degraded significantly due to the propagation of shear cracks. It demonstrate that it is important to consider the effect of the load level when assessing the contribution of shear deformation in RC beams.

5. Conclusion

In this paper, finite element analysis was conducted to investigate the contribution of shear deformation in RC shear-critical beams. A 2D concrete material model based on the smeared fixed crack theory was presented and incorporated into a commercial FEM software Abaqus through subroutine interface VUMAT. This model took into consideration the following characteristics of concrete: (1) biaxial failure criteria; (2)

the reduction of compressive strength due to orthogonal tensile strain; (3) the variable shear retention factor and shear strength at the crack dependent on the crack opening displacement; (4) The energy-based softening branch of uniaxial stress-strain relations of both compression and tension. A method of calculating the flexure and shear deformation separately out of the total deformation in the shear span was presented and implemented in the FEM model. The proposed FEM model and the deformation-separation method was validated by comparing the numerical simulations with experimental results of several RC shear-critical beams. The contribution of shear deformation in RC shear-critical beams, as well as the influence of several design parameters on it, was investigated. Based on the results shown in this paper, the following conclusions could be drawn:

(1) The mesh size sensitivity could be reduced when applying the presented energy-based softening branch to describing the compressive and tensile stress-strain relations.

(2) The FEM model combined with the proposed deformation-separation method could reproduce the total deformation, the shear deformation, the flexure deformation and crack patterns with reasonable accuracy for the beam specimens studied in this paper.

(3) In terms of the deformation-separation method presented in this paper, the number of the macro-elements into which the shear span was divided should be larger than the shear span-to-height ratio of the studied beam to obtain converged results. If not, the shear deformation could be overestimated.

(4) The shrinkage strain appears to be an important factor which may influence the cracking load and deformational behaviour, including both the flexure deformation and the shear deformation, of RC beams.

(5) For RC shear-critical beams without shear reinforcement, the deformational behaviour was governed by flexure because failure occurred soon after the formation of 'critical diagonal cracks'. No evident shear cracks could be seen before 'critical diagonal cracks' formed.

(6) For RC shear-critical beams with shear reinforcement, the shear deformation was not negligible after shear cracking. For the lower longitudinal reinforcement ratio, the lower shear reinforcement ratio, the lower shear span-to-depth ratio and the higher load level, the contribution of shear deformation could be more significant.

It should also be noted that flexure deformation defined in this paper was in fact the deformation induced by mean curvature which not only consisted of the flexure deformation based on Navier-Bernoulli theory but also the additional flexure deformation caused by shear cracks (Debernardi & Taliano, 2006; Ueda, et al., 2002). If the nominal shear deformation was defined as the total deformation minus the flexure deformation based on Navier-Bernoulli theory, the contribution of this nominal shear deformation could be even larger than that obtained in this study. That was why the formula proposed by ACI (2014) could strongly underestimate the deformation (Desalegne & Lubell, 2012).

Future work

As mentioned in the introduction, very few experiments have been conducted to measure the shear deformation in the shear span of RC shear-critical beams. With the help of digital image correlation (DIC) techniques, the displacement field on the surface of the shear span could be measured. Further experimental investigations are recommended in which the DIC techniques will be employed to measure the shear deformation and what's more, the strain field in the shear span. These experimental results not only are useful for studying the contribution of shear deformation in RC shear-critical beams but also can provide more comprehensive experimental results for calibrating and validating FEM models.

Acknowledgements

The authors gratefully acknowledge financial support from National Natural Science Foundation of China (No. 51378104) and A Project Funded by the Priority Academic Program Development of Jiangsu Higher Education Institutions. The work was made possible through contributions from the Development Fund of the Swedish Construction Industry, SBUF, ID:13010, the Swedish Research Council Formas, No 2012-1037 and Elsa and Sven Thysell Foundation.

References

AASHTO. (2007). AASHTO LRFD Bridge Design Specifications, 4th ed. Washington, DC: AASHTO.

ACI. (2014). Building Code Requirements for Structural Concrete (ACI318M-14) and Commentary. Farmington (MI): American Concrete Institute.

Bazant, Z. P., & Gambarova, P. (1980). Rough Cracks in Reinforced Concrete. *ASCE Journal of the Structural Division, 106*(ST4), 819-842.

Bazant, Z. P., & Oh, B. H. (1983). Crack Band Theory for Fracture of Concrete. *Materials and Structures, 16*(93), 155-177.

Belarbi, A., & Hsu, T. T. C. (1995). Constitutive Laws of Softened Concrete in Biaxial Tension-compression. *ACI Structural Journal, 92*(5), 562-573.

Bentz, E. C., Vecchio, F. J., & Collins, M. P. (2006). Simplified Modified Compression Field Theory for Calculating Shear Strength of Reinforced Concrete Elements. *ACI Structural Journal*, *103*(4), 614-624.

Bertagnoli, G., & Carbone, V. I. (2008). A Finite Element Formulation for Concrete Structures in Plane Stress. *Structural Concrete, 9*(2), 87-99.

Bertagnoli, G., Mancini, G., Recupero, A., & Spinella, N. (2011). Rotating Compression Field Model for Reinforced Concrete Beams under Prevalent Shear Actions. *Structural Concrete, 12*(3), 178-186.

Bresler, B., & Scordelis, A. C. (1963). Shear Strength of Reinforced Concrete Beams. *ACI Journal*, *60*(1), 51-74.

CEB-FIP. (1993). CEB-FIP Model Code 1990: Comite Euro-International du Beton.

CEN. (2004). Eurocode 2: Design of Concrete Structures-Part 1-1: General Rules and Rules for Buildings. Brussels: CEN.

Cervenka, J., & Cervenka, V. (2010). *On the Uniqueness of Numerical Solutions of Shear Failure of Deep Concrete Beams: Comparison of Smeared and Discrete Crack Approaches.* Paper presented at the Euro-C.

Cervenka, J., & Papanikolaou, V. K. (2008). Three Dimensional Combined Fracture-Plastic Material Model for Concrete. *International Journal of Plasticity, 24*(12), 2192-2220.

Cervenka, V. (1985). Constitutive Model for Cracked Reinforced Concrete. *ACI Journal Proceeding, 82*(6), 877-882.

Cervenka, V., & Pukl, R. (1992). *Computer Models of Concrete Structures*. Paper presented at the IABSE, Zurich, Switzerland.

Chen, G. M., Teng, J. G., Chen, J. F., & Xiao, Q. G. (2015). Finite Element Simulation of IC Debonding in FRP-Plated RC Beams: A Dynamic Approach. *Computers & Structures, 158*(1), 167-183.

Coronelli, D., & Mulas, M. G. (2006). Modeling of Shear Behavior in Reinforced Concrete Beams. *ACI Structural Journal, 103*(3), 372-382.

Crisfield, M. A., & Wills, J. (1989). Analysis Of R/C Panels Using Different Concrete Models. *Journal of Engineering Mechanics, 115*(3), 578-597.

Darwin, D., & Pecknold, D. A. (1977). Nonlinear Biaxial Stress-strain Law for Concrete. *Journal of the Engineering Mechanics Division, 103*(EM4), 229-241.

Debernardi, P. G., Guiglia, M., & Taliano, M. (2011). Shear Strain in B-Regions of Beams in Service. *Engineering Structures*, *33*(2).

Debernardi, P. G., & Taliano, M. (2006). Shear Deformation in Reinforced Concrete Beams with Thin Web. *Magazine of Concrete Research, 58*(3), 157-171.

Desalegne, A. S., & Lubell, A. S. (2012). Consideration of Shear Deformations for Slender Concrete Beams. *Special Publication, 284*(1), 1-18.

FIB. (2010a). *fib Model Code for Concrete Structures 2010*. Germany: Ernst & Sohn.

FIB. (2010b). Shear and Punching Shear in RC and FRC elements. Switzerland: International Federation for Structural Concrete.

Gribniak, V., Cervenka, V., & Kaklauskas, G. (2013). Deflection prediction of reinforced concrete beams by design codes and computer simulation. *Engineering Structures*, *56*, 2175-2186. doi: 10.1016/j.engstruct.2013.08.045

Hansapinyo, C., Pimanmas, A., Maekawa, K., & Chaisomphob, T. (2003). Proposed Model of Shear Deformation of Reinforced Concrete Beam after Diagonal Cracking. *Journal of Materials Concrete Structure Pavements, JSCE, 58*(1), 305-319.

Hendriks, M., Uijl, J. A. d., Boer, A. d., Feenstra, P. H., Belletti, B., & Damoni, C. (2012). Guidelines for Nonlinear Finite Element Analysis of Concrete Structures. Rijkswaterstaat-Ministerie van Infrastructuur en Milie.

Hibbitt, K. (1997). *ABAQUS: User's Manual*: Hibbitt, Karlsson & Sorensen, Incorporated.

Huang, Z., Lü, Z., & Tu, Y. (2016). Secondary development of ABAQUS based on disturbed stress field model (DSFM) and its comparison with damage plasticity model. *Tumu Gongcheng Xuebao/China Civil Engineering Journal, 49*(5), 40-49.

Huang, Z., Tu, Y., Grip, N., Sabourova, N., Bagge, N., Blanksvard, T., et al. (2016). *Modelling of Damage and its use in Assessment of a Prestressed Concrete Bridge*. Paper presented at the 19th IABSE Congress Stockholm, Stockholm, Sweden.

Jin, F. f. (2016). *Time-Dependent Behaviour of RC Beams Strengthened with Pre-stressed CFRP Straps.* Cambridge University, UK.

Kaklauskas, G., Gribniak, V., Bacinskas, D., & Vainiunas, P. (2009). Shrinkage influence on tension stiffening in concrete members. *Engineering Structures, 31*(6), 1305-1312. doi: 10.1016/j.engstruct.2008.10.007

Kent, D. C., & Park, R. (1971). Flexural Members with Confined Concrete. *Journal of the Structural Division 97*(ST7), 1969 - 1990.

Kim, J. H., & Mander, J. B. (2007). Influence of transverse reinforcement on elastic shear stiffness of cracked concrete elements. *Engineering Structures, 29*(8), 1798-1807.

Kim, K. S. (2004). *Shear Behavior of Reinforced Concrete Beams and Prestressed Concrete Beams.* University of Illinois at Urbana-Champaign, Urbana, USA.

Kupfer, H., & Gerstle, K. N. (1973). Behavior of Concrete Under Biaxial Stresses. *Journal of Engineering Mechanics, 99*(4), 852-866.

Maekawa, K., Pimanmas, A., & Okamura, H. (2003). *Nonlinear Mechanics of Reinforced Concrete*. London: Spon Press.

Malm, R. (2006). *Shear cracks in concrete structures subjected to in-plane stresses.* Royal Institute of Technology (KTH), Stockholm.

Nakamura, H. (2001). *Compressive Fracture Energy and Fracture Zone Length of Concrete.* Paper presented at the Modeling of Inelastic Behavior of RC Structures under Seismic Loads.

Pan, Z. F., Li, B., & Lu, Z. T. (2014). Effective shear stiffness of diagonally cracked reinforced concrete beams. *Engineering Structures, 59*(1), 95-103.

Rots, J. G. (1988). *Computational Modeling of Concrete Fracture.* PhD Theis, Delft University of Technology.

Sato, Y., Tadokoro, T., & Ueda, T. (2004). Diagonal Tensile Failure Mechanism of Reinforced Concrete Beams. *Journal of Advanced Concrete Technology 2*(3), 327-341.

Timoshenko, S., & Gere, J. (1972). *Mechanics of Materials*. New York: D. Van Nostrand Company.

Ueda, T., Sato, Y., Ito, T., & Nishizone, K. (2002). Shear Deformation of Reinforced Concrete Beam. *Journal of Materials Concrete Structure Pavements, JSCE, 56*(1), 9-23.

Van Mier, J. G. M. (1986). Multiaxial strain-softening of concrete. [journal article]. *Materials and Structures, 19*(3), 179-190. doi: 10.1007/bf02472034

Vecchio, F. (1982). *The Response of Reinforced Concrete to in-Plane Shear and Normal Stresses.* University of Toronto, Toronto.

Vecchio, F., & Collins, M. (1993). Compression Response of Cracked Reinforced Concrete. *Journal of Structural Engineering, 119*(12), 3590-3610. doi: doi:10.1061/(ASCE)0733-9445(1993)119:12(3590)

Vecchio, F. J. (1989). Nonlinear Finite Element Analysis of Reinforced Concrete Membranes. *ACI Structural Journal, 86*(10), 26-35.

Vecchio, F. J. (2004). Crack Shear-Slip in Reinforced Concrete Elements. *Journal of Advanced Concrete Technology, 2*(3), 289-300.

Vecchio, F. J., & Collins, M. P. (1986). The Modified Compression-Field Theory for Reinforced-Concrete Elements Subjected to Shear. *ACI Journal, 83*(2), 219-231.

Vecchio, F. J., & Shim, W. (2004). Experimental and Analytical Reexamination of Classic Concrete Beam Tests. *Journal of Structural Engineering, 130*(3), 460-469.

Wang, T., Dai, J. G., & Zheng, J. J. (2015). Multi-Angle Truss Model for Predicting the Shear Deformation of RC Beams with Low Span-Effective Depth Ratios. *Engineering Structures, 91*(15), 85-95.

Zhu, R. H., Hsu, T. T. C., & Lee, J. Y. (2001). Rational Shear Modulus for Smeared Crack Analysis of Reinforced Concrete. *Structural Journal of the American Concrete Institute, 98*(4), 443-450.

Table 1 Details of beam specimens

Reference	Beam	f_c (MPa)	$b\times h$ (mm)	a/d	Bottom Steel	Top Steel	Stirrup
Debernardi and Taliano (2006)	DT-TR6	35.6	100*×600	4.1	9D16	3D12	D8@200
Hansapinyo, et al. (2003)	HP-S1	33.0	150×350	2.6	4D25	2D25	D6@80
	HP-S2	33.0	150×350	3.5	4D25	2D25	D6@80
	HP-S3	33.0	150×350	2.6	2D25	2D25	D6@80
	HP-S4	33.0	150×350	2.6	2D25	2D25	D6@120
Bresler and Scordelis (1963)	BS-OA1	22.6	305×552	3.9	4No.9	None	None
	BS-OA2	23.7	305×552	4.9	5No.9	None	None
	BS-A1	24.1	305×552	3.9	4No.9	2No.4	No.2@210
	BS-A2	24.3	305×552	4.9	5No.9	2No.4	No.2@210
	BS-B1	24.8	229×552	3.9	4No.9	2No.4	No.2@190
	BS-B2	23.2	229×552	4.9	4No.9	2No.4	No.2@190
	BS-C1	29.6	152×552	3.9	2No.9	2No.4	No.2@210
	BS-C2	23.8	152×552	4.9	4No.9	2No.4	No.2@210

*For DT-TR6, b refers to the web width

Table 2. Material properties of the reinforcement

Reference	Reinforcement	Area (mm^2)	f_y (MPa)
Debernardi and Taliano (2006)	D8	50	570
	D12	113	540
	D16	201	540
Hansapinyo, et al. (2003)	D6	28	370
	D25	490	440
Bresler and Scordelis (1963)	No. 2	32.2	325
	No. 4	127	345
	No. 9	645	555

Figure 1. Uniaxial stress-strain relations of concrete; (a) compressive stress-strain curve; (b) tension softening.

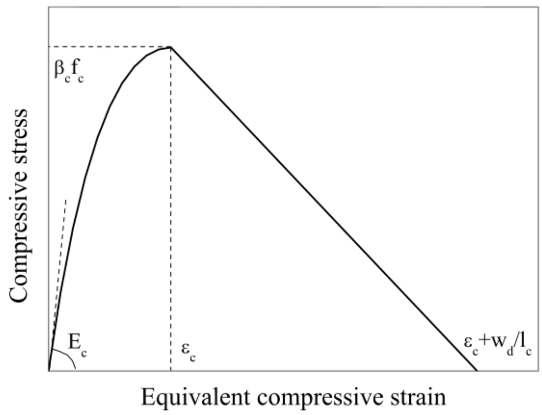

(a)

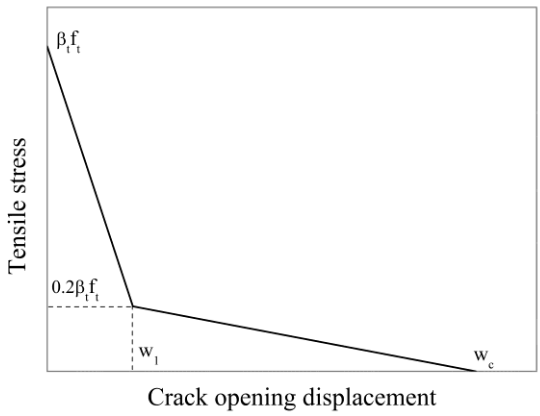

(b)

Figure 2. Biaxial failure criteria of concrete.

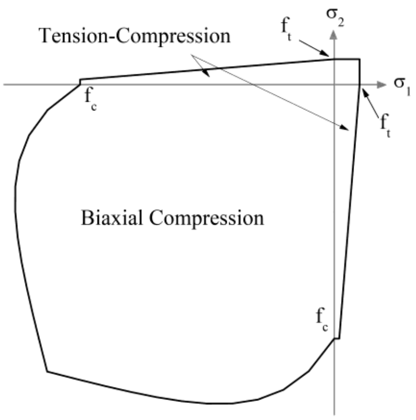

Figure 3. The method of calculating the shear deformation in the FEM model; (a) macro-element; (b) the division of the shear span.

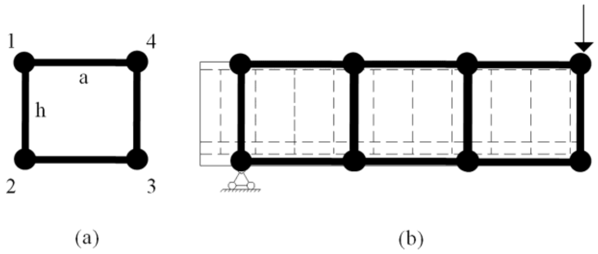

Figure 4. Details of DT and HP series beams

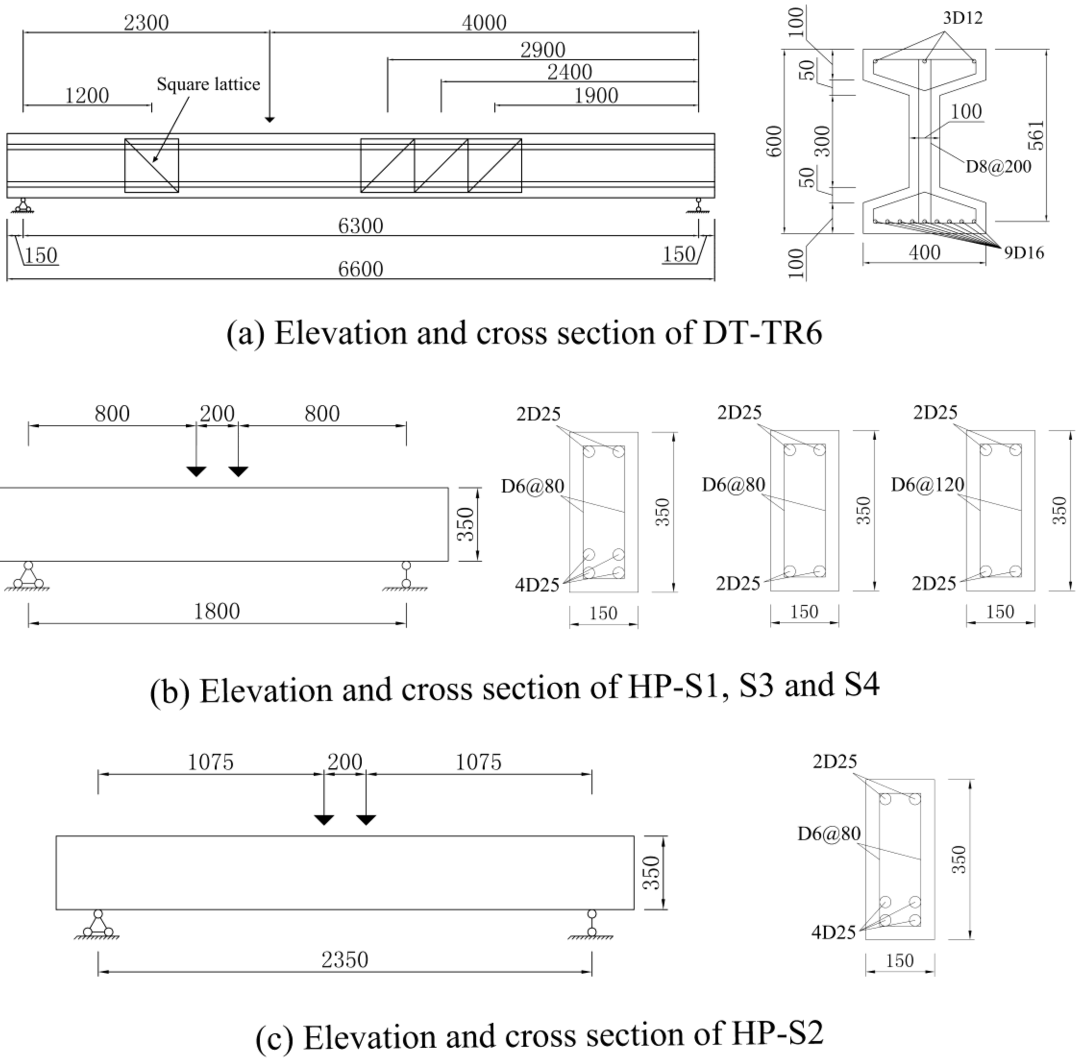

(a) Elevation and cross section of DT-TR6

(b) Elevation and cross section of HP-S1, S3 and S4

(c) Elevation and cross section of HP-S2

Figure 5. Calculated load-displacement curves of DT-TR6 with elements of different sizes

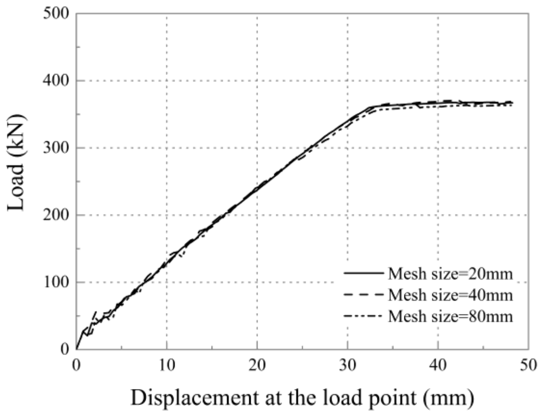

Figure 6. Calculated contributions of shear deformation with different numbers of macro-elements

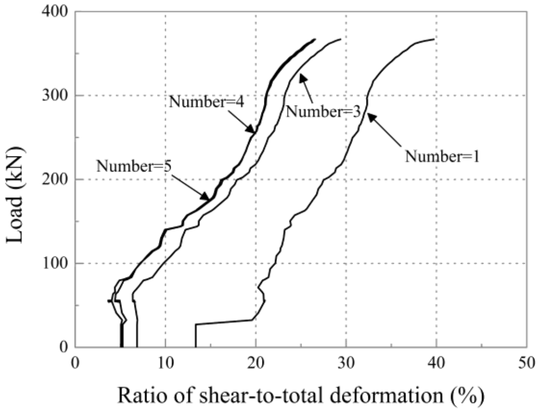

(a) DT-TR6 (*a/h*=3.8)

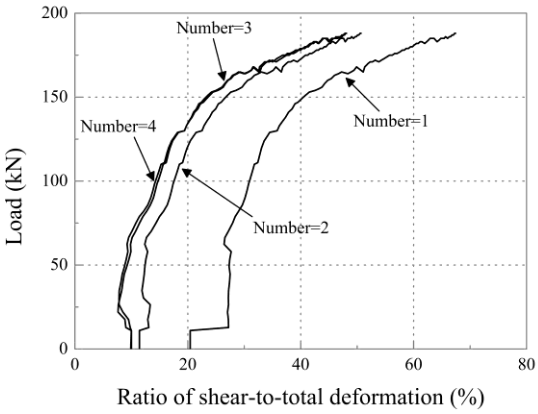

(b) HP-S1 (*a/h*=2.3)

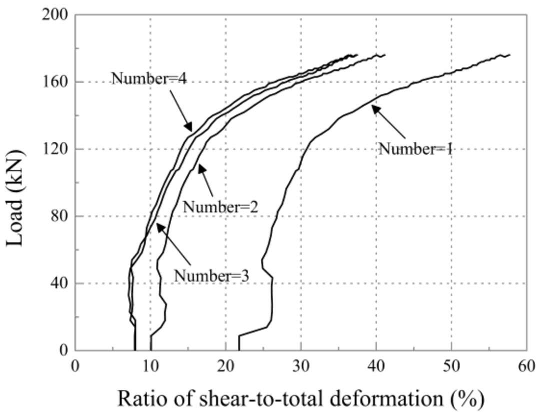

(c) HP-S2 (*a/h*=3.0)

Figure 7. Load displacement curves for DT-TR6

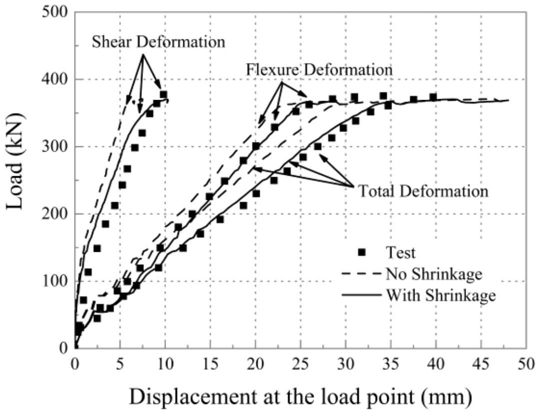

Figure 8 Load displacement curves for HP series beams

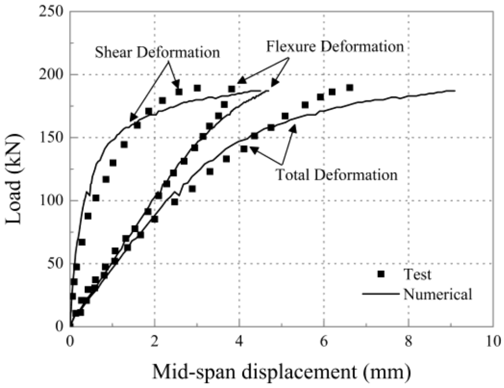

(a) HP-S1

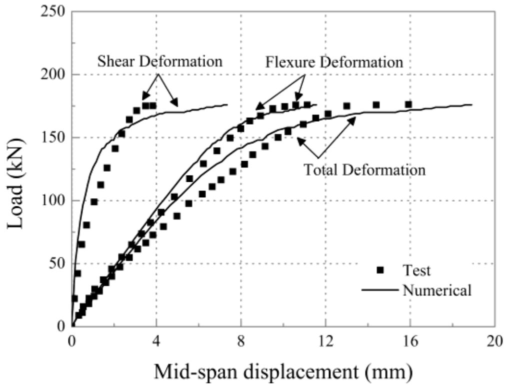

(b) HP-S2

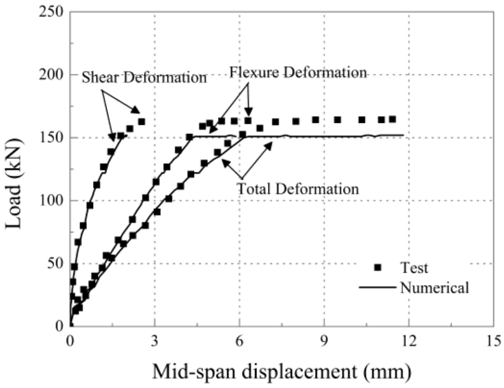

(c) HP-S3

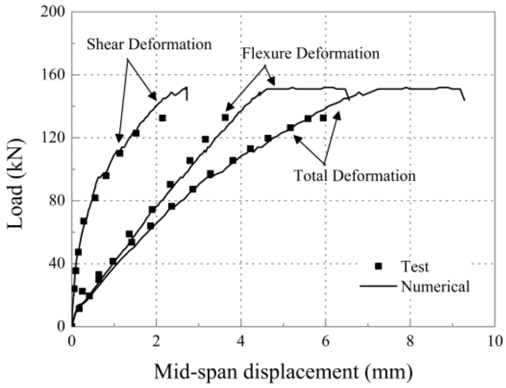

(d) HP-S4

Figure 9 Flexure deformation and shear deformation for HP series beams

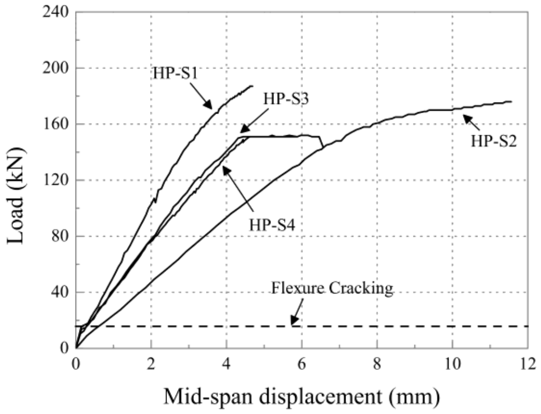

(a) Flexure deformation

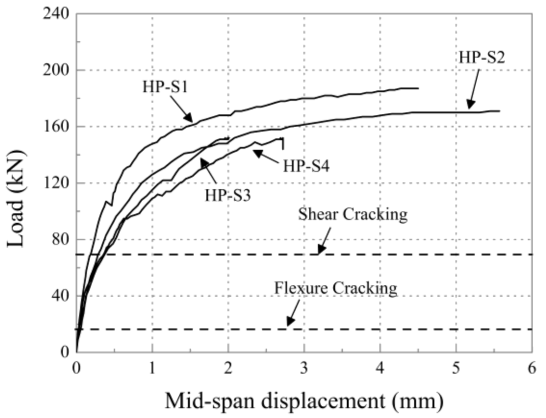

(b) Shear deformation

Figure 10 Calculated contributions of shear deformation for DT and HP beams

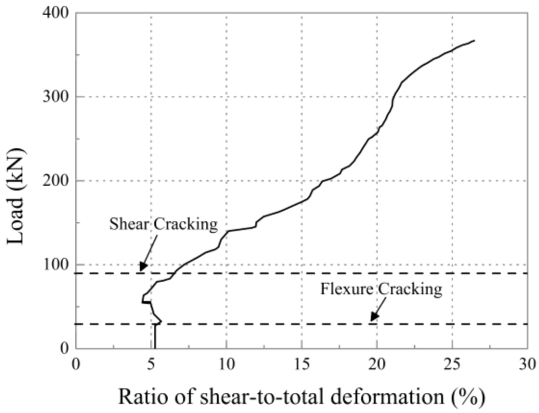

(a) DT-TR6

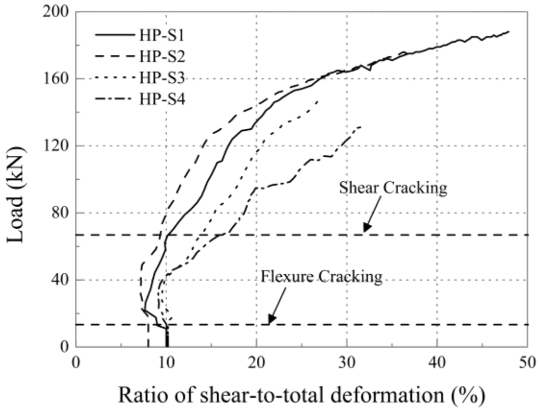

(b) HP series beams

Figure 11 Details of three BS beams

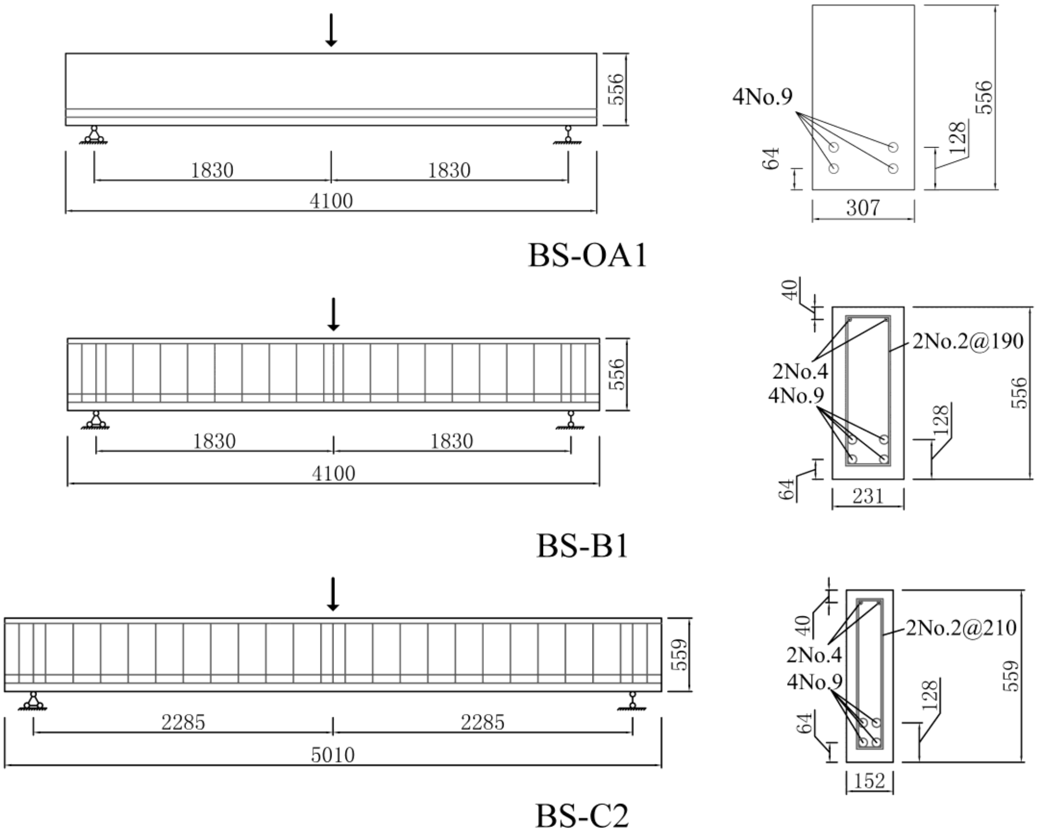

Figure 12 Load displacement curves for BS series beams

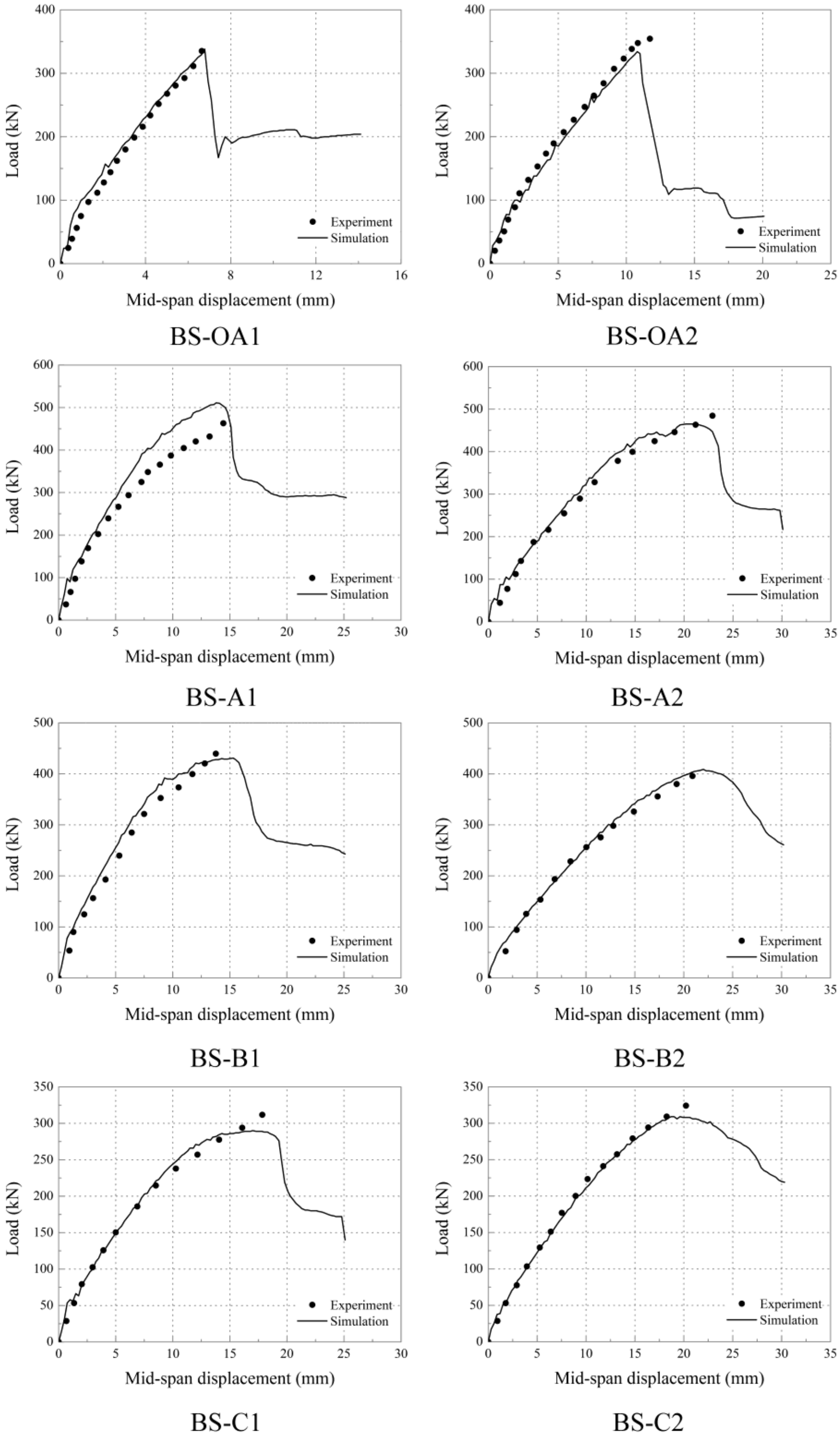

Figure 13 Crack patterns at failure for BS series beams

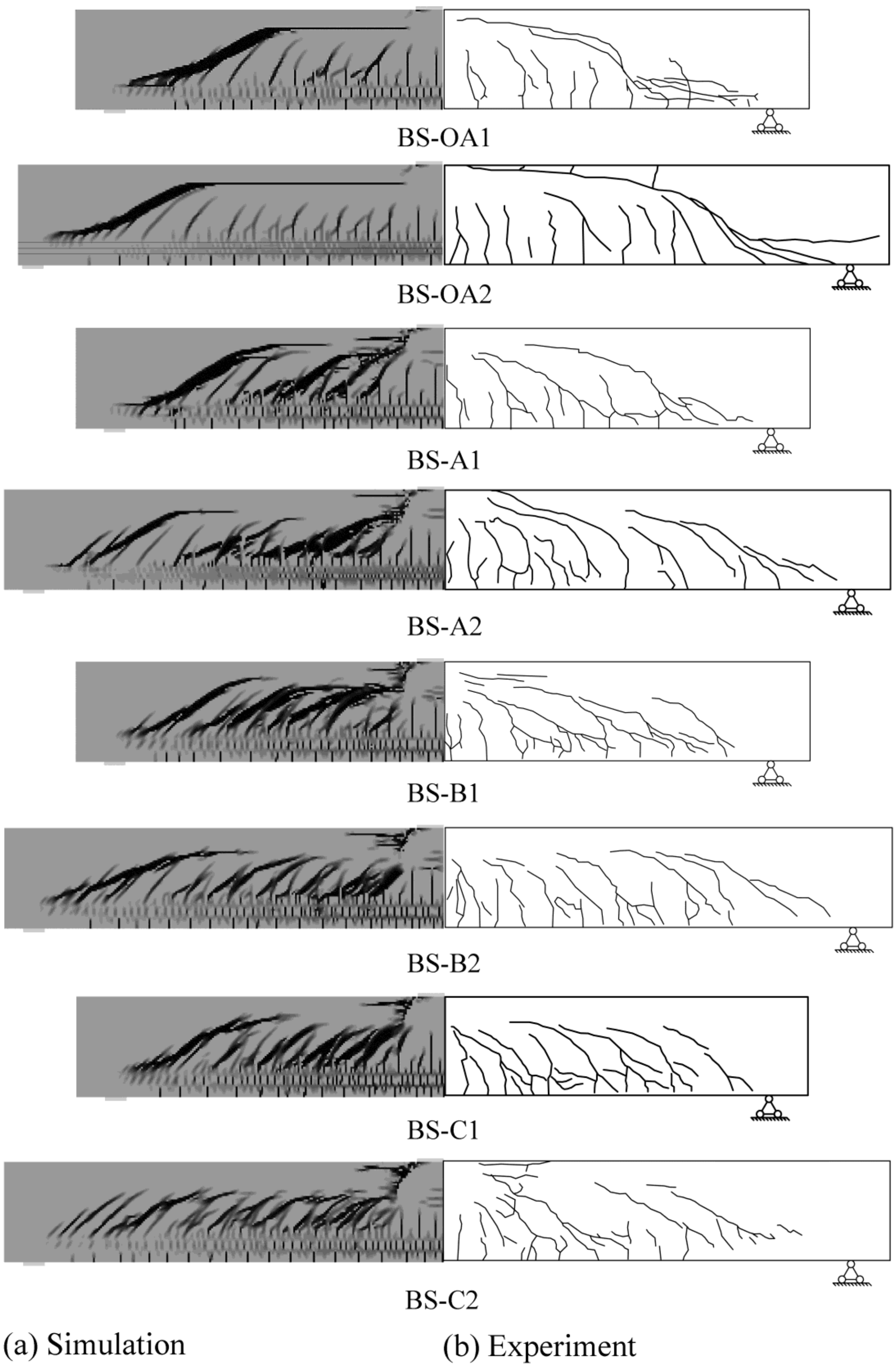

Figure 14 Calculated contributions of shear deformation for BS-OA2 and BS-A2

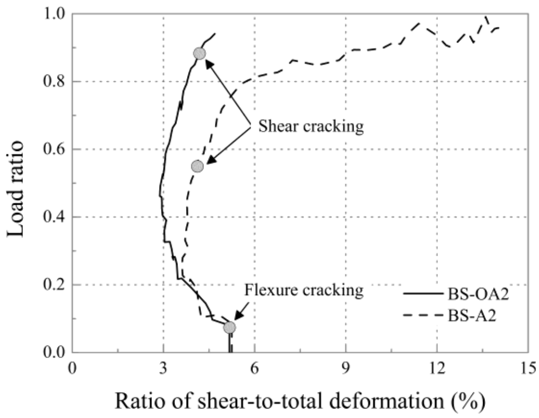

Figure 15 Calculated contributions of shear deformation for BS-B1 and BS-B2

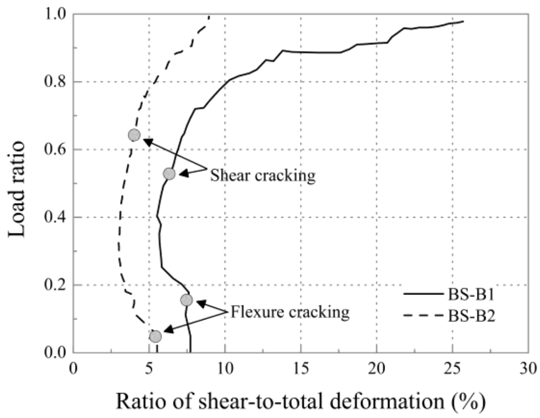

Figure 16 Calculated contributions of shear deformation for BS-C1 and DT-TR6